Solar Energy 271 (2024) 112414

Contents lists available at ScienceDirect

Solar Energy

journal homepage: www.elsevier.com/locate/solener

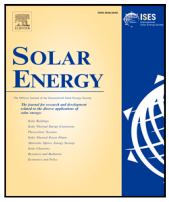

A metaheuristic-based method for photovoltaic temperature computation under tropical conditions

Liomnis Osorio [a,b], Mailyn Moreno [c], Marco Rivera [d,e], Víctor Tuninetti [f,*], Gerardo Ruíz Chavarria [g], Laurent Duchêne [b], Patrick Wheeler [h]

[a] Engineering Doctoral Program, Universidad de La Frontera, Francisco Salazar 01145, Temuco, 4780000, Chile
[b] ArGEnCo Department, MSM team, University of Liège, Quartier Polytech 1, allée de la Découverte 9, Liège, 4000, Belgium
[c] Departamento Administración, Facultad de Economía y Administración, Universidad Católica del Norte, Av. Angamos 0610, Antofagasta, 1270398, Chile
[d] Laboratorio de Conversión de Energías y Electrónica de Potencia (LCEEP), Dirección de Investigación, Universidad de Talca, Merced 437, Curicó, 3341717, Chile
[e] Power Electronics, Machines and Control Research Group, Faculty of Engineering, University of Nottingham, 15 Triumph Rd, Lenton, Nottingham NG7 2GT, United Kingdom
[f] Department of Mechanical Engineering, Universidad de La Frontera, Francisco Salazar 01145, Temuco, 4780000, Chile
[g] Facultad de Ciencias, Universidad Nacional Autónoma de Mexico, Ciudad de Mexico, 04510, Mexico
[h] Faculty of Engineering, University of Nottingham, 15 Triumph Rd, Lenton, Nottingham NG7 2GT, United Kingdom

ARTICLE INFO

Keywords:
Photovoltaic efficiency
Photovoltaic module temperature
Restart local search algorithm
NOCT model

ABSTRACT

Tropical climates have favorable irradiation levels for the development of photovoltaic systems; however, high temperatures have a negative impact on the efficiency of solar cells. Since direct measurement of cell temperature is not common, mathematical models are needed to make predictions. Numerous models have been documented, highlighting the challenge of applying a universal model to different climatic conditions. The main contribution of this study is the proposal of a metaheuristic algorithm to accurately compute the temperature of solar cells. This method is simple and effective in exploring numerous potential states of the reference parameters (i.e., irradiance and ambient temperature). Data collected over a 23-month period in two photovoltaic installations with an output power of 2.2 MW of multicrystalline silicon technology were used to develop the proposed method and validate it. The proposed model was compared with 19 previously reported models in the literature. Compared to the model recommended by the International Electrotechnical Commission (IEC Standard 61215-1), the mean square error, mean absolute error (MAE) and mean absolute percentage error were reduced by 4.9, 4.8, and 2.4 times, respectively. The accuracy of the proposed method is demonstrated by MAE errors ranging from 0.56 °C to 1.88 °C, obtained by considering three different daily profiles of irradiance and ambient temperature. Therefore, the proposed method is recommended to more accurately calculate the temperature of the photovoltaic cell in tropical areas.

1. Introduction

According to the International Renewable Energy Agency, the expansion of the wind and solar energy generation sector in 2022 accounted for the largest annual increase in renewable energy generation capacity. These two sources accounted for 90% of all net renewable additions in 2022 [1]. Globally, all renewable energy sources contributed to a 295 GW (+9.6%) increase in capacity, with photovoltaic (PV) energy leading the expansion with a worldwide increase of 192 GW (+22%) [2]. .5

Regarding PV energy, silicon-based technologies continue to dominate the market and are expected to maintain their position for the next five years [3]. However, the electrical efficiency (η) of this technology is negatively affected when the PV cell temperature (T_c) exceeds 25 °C [4–6]. Other factors, such as the physical characteristics of the PV module (i.e., monocrystalline, multicrystalline or amorphous silicon technology), setup configuration, meteorological data (i.e., irradiance (G), ambient temperature (T_a), wind velocity (v_w)), and electrical parameters from the datasheet, must also be taken into account [7,8]. However, temperature is one of the most extensively studied parameters, as it has been identified as one of the most significant and influential factors on PV efficiency [9].

* Corresponding author.
E-mail address: victor.tuninetti@ufrontera.cl (V. Tuninetti).

https://doi.org/10.1016/j.solener.2024.112414
Received 11 November 2023; Received in revised form 25 January 2024; Accepted 15 February 2024
Available online 26 February 2024

Nomenclature

Acronyms

EVA	Ethyl Vinyl Acetate
IEC	International Electrotechnical Commission
MAE	Mean Absolute Error
MAPE	Mean Absolute Percentage Error
NOCT	Nominal Operating Cell Temperature
PV	Photovoltaic
RMSE	Root Mean Square Error
ROMT	Realistic Operational Module Temperature
STC	Standard Test Conditions
tFOC	Tropical Field Operation Cell Temperature

Symbols

α	transmissivity coefficient
β_{STC}	temperature coefficient of power (%/°C)
η	efficiency (%)
η_{STC}	efficiency at STC (%)
τ	absorbance coefficient
AM	air mass
e	estimated values
$E_{c,day}$	daily produced energy by photovoltaic cells
$E_{i,day}$	daily produced energy by photovoltaic installation
G	irradiance (W/m^2)
G_{NOCT}	irradiance at NOCT (W/m^2)
H	convective heat transfer coefficient (W/m^2 K)
H_r	relative humidity (%)
$Iter$	iteration
m	measured values
n	number of data
$P_{c,STC}$	power of PV cells at STC (W)
P_c	power of PV cells (W)
R^2	coefficient of determination
T_a	ambient temperature (°C)
T_c	cell temperature (°C)
$T_{a,NOCT}$	ambient temperature at NOCT (°C)
u_0	empirical coefficient (W/m^2)
u_1	empirical coefficient (W s/m^3 K)
v_w	wind velocity (m/s)
d	day
h	hour
m	month
y	year

1.1. Effect of temperature on silicon solar cell efficiency

The difference between T_c and T_a values can be estimated as a function of G, using the thermal conductivity of the PV module materials [4]. The solar cells operate under open space irradiation and, to protect them from harsh environmental conditions, they are encapsulated with additional materials such as tempered glass, ethyl vinyl acetate (EVA) and a polymer layer (back-sheet) [5,10]. Due to the structure and physical composition of PV modules, T_c is determined by the balance between the heat produced by the PV module and the heat lost to the environment (encapsulating material). The latter is mainly affected by T_a and v_w at the installation site [11]. PV module properties influence heat loss include thermal resistance, emissivity properties, and surface-related convection properties [12].

As a general rule, η is evaluated under the standard test conditions (STC) specified in the datasheet, which define $G = 1000$ W/m^2, $T_c = 25$ °C and air mass 1.5 AM. Under these conditions, the electrical parameters (current, voltage and power) are obtained with $\eta = f(G, T_c, AM)$. However, η is typically assessed without considering meteorological factors such as tropical, desert or extreme climates. To better approximate actual operating conditions, the datasheet also provides the Nominal Operating Cell Temperature (NOCT), defined as the cell temperature in a module exposed to $G = 800$ W/m^2, $T_a = 25$ °C and $v_w = 1$ m/s, with typical NOCT values ranging from 43 °C to 47 °C. In practice, both the STC and NOCT values are imprecise for many real-world PV installations [13,14].

Crystalline silicon cells have a correlation between T_c and η, expressed by Eq. (1) [15].

$$\eta = \eta_{STC}\left[1 + \beta_{STC}\left(T_c - T_{a,STC}\right)\right] \tag{1}$$

where η_{STC} is the reference electrical efficiency (%), β_{STC} is the reference temperature coefficient of the power, $T_{a,STC}$ is the reference cell temperature; η_{STC}, β_{STC} and $T_{a,STC}$ are available from the datasheet.

During the incident of irradiance on the PV module, a fraction of the energy causes a slight increase in the short-circuit current, while the rest is transformed into thermal energy. Consequently, T_c to increase and the open-circuit voltage to decrease, causing the power of cells P_c and η to decrease. Eq. (2) is one of the most commonly used to express the correlation between T_c and P_c [16].

$$P_c = P_{c,STC}\frac{G}{G_{STC}}\left[1 + \beta_{STC}\left(T_c - T_{a,STC}\right)\right] \tag{2}$$

where $P_{c,STC}$ is the reference power (W), is available from the datasheet. The amount of produced energy is highly dependent on the temperature during the day. The cumulative daily produced energy $E_{c,day}$ is given by Eq. (3) [17].

$$E_{c,day} = \frac{P_{c,STC}}{G_{STC}}\sum_{h=1}^{H} G_{(h,d,m,y)}\left[1 + \beta_{STC}\left(T_{c(h,d,m,y)} - T_{a,STC}\right)\right]\Delta t_h \tag{3}$$

where $T_{c(h,d,m,y)}$ is the cell temperature value at the time interval Δt_h of day d of month m of year y. T_c is essential to accurately predict η, P_c and $E_{c,day}$, therefore, it is important to conduct an investigation and implement appropriate mathematical models according to the specific case study.

1.2. PV module temperature estimation models – a literature review

Two categories of approaches and tools used to estimate T_c have been identified in the literature and categorized into steady-state and dynamic [11]. The thermal models based on steady-state are relatively simple and assume that all parameters are time-independent, while the dynamic thermal models are relatively complex, and require more computation time, because some parameters are time-dependent [18]. Since the turn of the century, numerous predictive models incorporating different climate factors and methodologies have been documented. Some approaches use the correlation $T_c = f(G, T_c)$ primarily, but to enhance the results, additional input variables such as v_w or relative humidity (H_r) can be added using the correlation $T_c = f(G, T_c, H_r, v_w)$.

These thermal models are intended to be useful for specialists interested in installing PV systems in their respective countries and nearby regions. In Europe, [4] analyzed 24 thermal models and found that the highest T_c were reached in the summer months; [35] proposed a transient one-dimensional thermal model that provides the distribution of T_c along the panel thickness, which is used to predict P_c; [36] developed a novel compact model to predict the coefficient f which relates T_c with G, T_a, v_w, the inclination of PV module and the output power P_c. In Asia, [33] derived a correlation between T_c, η and P_c, using a case study of a floating PV system of 200 GW; [37] suggested a predictive model to calculate P_c as a function of G, T_a, v_w, and

Table 1
Thermal models to calculate the operating cell temperature.

Year	Model	Reference	Equation
1976	$T_c = T_a + 0.03G$	[19]	(4)
1980	$T_c = T_a + \frac{G}{G_{NOCT}}\left(NOCT - T_{a,NOCT}\right)\left(1 - \frac{\eta_{STC}}{\alpha\tau}\right)$	[20]	(5)
1984	$T_c = 1.31T_a + 0.0282G - 1.65v_w + 3.81$	[21]	(6)
1985	$T_c = T_a + 0.028G - 1$	[22]	(7)
1986	$T_c = T_a + \frac{G}{G_{NOCT}}\left(NOCT - T_{a,NOCT}\right)$	[23]	(8)
1990	$T_c = 1.14\left(T_a - 25\right) + 0.0175\left(G - 300\right) + 30.006$	[24]	(9)
1996	$T_c = T_a + \frac{G}{1000}\left(0.0712v_w^2 - 2.411v_w + 32.96\right)$	[25]	(10)
1997	$T_c = T_a + \frac{G}{1000}\left(19.6e^{-0.223v_w} + 11.6\right)$	[26]	(11)
2003	$T_c = 0.943T_a + 0.028G - 1.528v_w + 4.3$	[27]	(12)
2004	$T_c = T_a + Ge^{-3.56-0.0750v_w}$	[28]	(13)
2004	$T_c = T_a + Ge^{-3.47-0.0594v_w}$	[28]	(14)
2006	$T_c = T_a + \left(\frac{9.5}{5.7 + 3.8v_w}\right)\frac{G}{G_{NOCT}}\left(NOCT - T_{a,NOCT}\right)\left(1 - \frac{\eta_{STC}}{\alpha\tau}\right)$	[29]	(15)
2007	$T_c = T_a + 0.031G$	[30]	(16)
2008	$T_c = T_a + \frac{0.25}{5.7 + 3.8v_w}G$	[31]	(17)
2008	$T_c = T_a + \frac{0.32}{8.91 + 2v_w}G$	[31]	(18)
2014	$T_c = 0.943T_a + 0.0195G - 1.528v_w + 0.3529$	[32]	(19)
2014	$T_c = T_a + \frac{G}{886}\left(tFOCT - 34\right)$	[14]	(20)
2018	$T_c = 0.9458T_a + 0.0215G - 1.2376v_w + 2.0458$	[33]	(21)
2020	$T_c = T_a + \left(\frac{\alpha\tau G(1 - \eta_{STC})}{2h}\right)$	[34]	(22)

T_a and G are measured by meteorological stations; $NOCT$, η_{STC}, $G_{NOCT} = 800$ W/m^2 and $T_{a,NOCT} = 20$ °C are given in the datasheet; $tFOCT = 45$ °C; $\alpha\tau = 0.9$ is the product of the transmissivity and absorbance coefficients; h - convective heat transfer coefficient, with $h = u_0 + u_1 v_w$; $u_0 = 12.85$ W/m^2; $u_1 = 1.06$ W s/m^3 K.

H_r, of the PV modules installed on a rooftop; [38] proposed two innovative models (one with and one without wind) to improve the accuracy of estimating T_c in outdoor conditions, taking into account the variation of G over time and the thermal inertia of different PV module technologies; [39] developed a novel model that determines T_c based on T_a, G and v_w. In Africa, [12] used an experimental technique to obtain datasets to develop 80 models, optimize 7 thermal models, and compute T_c at various tilt angles and orientations; [6] proposed a methodology to predict T_c using G and T_a as input parameters, for monocrystalline PV modules under a hot desert climate, based on actual and estimated meteorological data. In America, [32] obtained a model based on linear correlation with an error of less than 3%, for forecasting T_c under a tropical climate, based on T_a, G and v_w; [5] proposed a new model to calculate the thermal behavior of PV modules with an accuracy of a mean absolute percentage error of 3.1%, based on the analysis of a 172-day database; [40] estimated and compared T_c of a floating PV module using thermal, empirical and computational fluid dynamics (CFD) models.

These aforementioned models highlight the absence of a universally accepted model applicable to multiple climatic environments. Based on the empirical models of 1976–2018 analyzed by [41], in addition to the models obtained by [14,34], 19 empirical thermal models were examined in this paper, as summarized in Table 1.

The specialists in Cuba use the model represented by Eq. (8) in Table 1 to calculate the operating temperature of PV cells, which leads to the prediction of PV produced energy. This model is known as the NOCT model and is recommended by the IEC Standard 61215-1 to predict the cell temperature of the entire module [42]. However, the NOCT model is not effective when applied to different meteorological conditions found in different locations around the world. [13] proposed modifying this model by introducing a new condition called Realistic Operational Module Temperature (ROMT) to better distinguish it from NOCT. [14] also proposed a new condition called Tropical Field Operation Cell Temperature (tFOCT) for the tropical climate of Malaysia (Eq. (20) listed in Table 1) instead of the NOCT condition, with the values of $G_{tFOCT} = 886$ W/m^2 and $T_{a,tFOCT} = 34$ °C.

1.3. Metaheuristics for finding a path

Metaheuristics are well known as approximate methods for optimizing functions in large solution spaces or domains. While they do not guarantee to find the global optimum, they typically obtain sufficiently good solutions in a reasonable period of time [43]. Metaheuristics have been widely used in various fields, including combinatorial optimization, artificial intelligence, planning, engineering, and data science [44]. These techniques have proven to be effective in solving complex optimization problems where finding the best possible solution is challenging or impractical within a reasonable time frame.

The key characteristic of metaheuristics, which grants them their general nature, is that they do not make assumptions about the problem being addressed or the objective function being optimized. They only require a defined way to represent and evaluate solutions, as well as operators to construct an initial solution and transform the solutions into new ones [43].

Some examples of metaheuristics include simulated annealing, tabu search, and evolutionary algorithms. In recent years, many new metaheuristics, variants, and combinations of existing ones have emerged. These techniques have been successfully applied to problems such as resource allocation, scheduling, route optimization, parameter optimization, and design problem solving [45].

1.4. Tropical climate and current status of PV installations in Cuba

Cuba has a predominantly warm tropical climate with a rainy season in the summer [46]. In 2022, the Cuban Institute of Meteorology reported an extremely hot year, with a mean annual $T_a = 25.5$ °C, representing an increase of 0.88 °C compared to the previous historical record (2021), confirming the trend of rising temperatures [47].

In 2014, the Cuban government declared its intention to transit to a more diverse energy mix through the Prospective Development of Renewable Energy Sources and the Efficient Use of Energy for 2014–2030. The focus is on increasing the share of renewable energy sources [48]. The goal is to achieve an 24% of electricity from renewable sources by 2030 [49], with a contribution from the PV capacity of 700 MW [50]. Currently, the installed capacity in Cuba is 258 MW [2]. Domestically

produced (model DSM-270) and imported PV modules from various manufacturers and power capacities are utilized, but only 37% of the total capacity planned for 2030 has been achieved so far.

While the meteorological conditions in this region are favorable for PV energy development, with a daily average insolation of approximately 5 kWh/m^2 on a horizontal surface [51], the continuous exposure to intense solar radiation in the tropical climate leads to an increase in the cell temperature, resulting in a decrease in efficiency η and maximum power point P_c. Given that 63% of PV systems are yet to be designed, sized, and installed, it is crucial to utilize thermal models for accurate calculations of their short-, medium-, and long-term performance, as well as the annual electrical energy production.

In this context, the goal of the study is to propose a metaheuristic-based method to calculate the operating temperature using the correlation $T_c = f(G, T_a)$. A more appropriate and representative NOCT model is desired for tropical meteorological conditions. To achieve it, a steady-state approach based on the Occam razor principle is used, which asserts that when there are multiple possible explanations for a phenomenon, the simplest one is often correct [52]. This approach represents the original contribution of the study and can be applied in any geographical area, provided that accurate measurements are available and collected over a period of at least one year. For this study, measurements from two operational PV plants in eastern Cuba were used, combined with data from the Cuban Institute of Meteorology and technical specifications of PV modules.

The structure of this paper is as follows: Section 2 describes the steps taken to develop the method, introducing local search as one of the most promising metaheuristic algorithms for this study. The flowchart of the proposed metaheuristic-based method is also presented. Section 3 presents and discusses the advantages of the proposed method, comparing it with 19 previously established empirical models. Finally, Section 4 objectively summarizes the main results and contributions.

2. Materials and methods

The cell temperature was computed using the approach based on the NOCT model described by Eq. (8) listed in Table 1. Despite the recommendation of IEC Standard 61215-1, it would be more useful to develop a new model that improves the correlation between T_c, T_a and G, considering the data of the specific meteorological conditions of the PV installation.

2.1. Specifications of the PV installations

The data of G, T_a, and T_c from two PV installations connected to the National Electroenergetic System in the eastern zone of Cuba were analyzed. Each PV installation is composed of 8,800 modules, which provides an installed capacity of 2.2 MW.

Table 2 shows the technical specifications of the PV modules DSM-270 [53] and JKM265PP [54], both certified according to the IEC Standard 61215 [42]. The setup is arranged on metal structures on the ground, with air circulation behind the back-sheet (free-standing PV modules).

The PV systems were equipped with a SunGrow SolarInfo^{TM}EM environmental monitoring device with integrated sensors to measure irradiance, temperature (T_a and T_c), and wind velocity. Based on the technical specifications, the irradiance sensor has a sensitivity of 7 ~ 14 μv/W m^{-2}, a spectral range of 300 ~ 3000 nm, an annual stability of ±2%, and an output range of 0 ~ 2000 W/m^2; the ambient and PV cell temperature sensor has the same technical characteristics, with an accuracy of ±0.1 °C for the range of −55 ~ +125 °C; to measure the PV cell temperature values, the sensor was tightly connected onto the back sheet of the module to ensure close contact; the wind velocity sensor has an accuracy of 0.1 m/s (per 5 m/s) for the measurement range of 0 ~ 96 m/s.

Table 2
Technical specifications of the PV modules.

	PV module	
Parameter	DSM-270	JKM265PP
P_{mpp} (W)	270 ± 3%	265 ± 3%
η_{STC} (%)	16	16.19
β_{STC} (%/°C)	−0.41	−0.40
Number of cells	60 (6 × 10)	
Operating temperature (°C)	−40 ~ +85	
$NOCT$ (°C)	45 ± 2	
Top side	Tempered glass	
Encapsulating material	EVA	
Cell type	Multicrystalline	

2.2. Datasets and preprocessing data

Metaheuristics do not necessarily require data cleaning; however, it is essential to apply a data filter to ensure the consistency with previously recorded measurements. Following this procedure ensure that the data are representative and contextually relevant, enhancing the accuracy of the findings [55]. Consequently, recovery of data lost was not necessary in this study.

The measurement period was from January 1, 2021 to December 19, 2022 with a 10-minute resolution. Some measurements were not registered, due to technical issues with the environmental monitoring device. The datasets consist of a matrix of 93206 × 3 and 93914 × 3 for the DSM-270 and JKM265PP PV modules, respectively. According to the criteria for NOCT conditions [42] and studies conducted by [13,56], the nominal operating temperature can be determined by rejecting the following measurements:

- Wind velocity outside of range: v_w = 0.25–1.75 m/s.
- Ambient temperature outside the range: T_a = 5–35 °C.
- Values of irradiance: G < 400 W/m^2.
- Variations of G between successive 10-minute intervals: ΔG > 10%.
- Variations of v_w between successive 10-minute intervals: Δv_w > 4 m/s.
- Variations of T_a between successive 10-minute intervals: ΔT_a > 5 °C.

After filtering the measured data according to the criteria described above, datasets of 655 × 3 and 1168 × 3 were obtained, for DSM-270 and JKM265PP PV modules, respectively. These results represent 0.98% of the measurements that comply with the NOCT conditions. Therefore, it is advisable to use a model that responds better to the environmental conditions of the PV installations. A similar result was obtained by [13], with 0.02% of data filtered of a dataset of 219168 measurements.

Based on the report by [47] of the Cuban Institute of Meteorology, a range of T_a = 2.80–36.90 °C was defined for data preprocessing. This criterion was used as the limits to avoid possible errors in the temperature measurement. Additionally, a condition of $G \geq 100$ W/m^2 was applied to exclude night-time measurements and to account for fluctuations in irradiance caused by transient cloudiness, which is common during summer periods. Finally, the dataset consisting of two matrices of size 28304 × 3 and 39069 × 3 were obtained for the DSM-270 and JKM265PP PV modules, respectively.

Fig. 1(a) shows the plot of the measured irradiance, with three peaks from 120–420 W/m^2, 450–690 W/m^2 and 720–990 W/m^2; the values above 1000 W/m^2 have a low probability, while the measured maximum value was 1199.60 W/m^2 with the lowest probability. Figs. 1(b) and 1(c) show the plot for T_a and T_c; the probable temperature ranges are 25–35 °C and 22–48 °C, respectively. The maximum values registered were T_a = 35 °C (Fig. 1(b)) and T_c = 57.10 °C (Fig. 1(c)). Registered measurements that comply with the condition of $T_a > T_c$ indicate that no PV energy is generated due to very low levels of

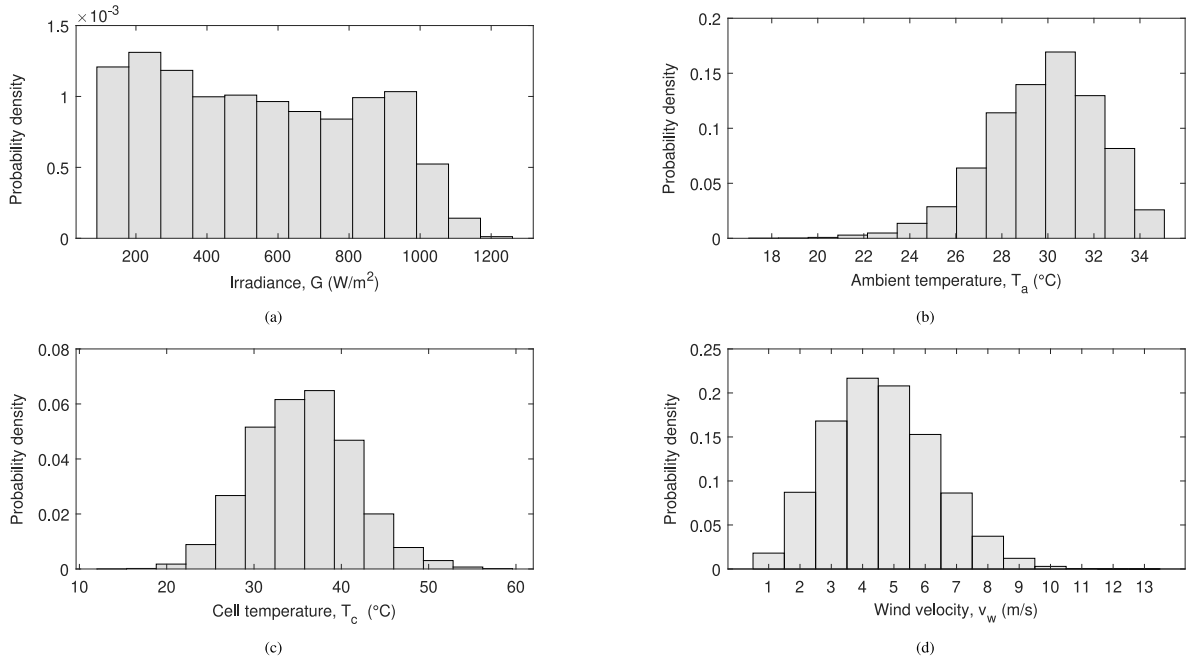

Fig. 1. Plots of probability density of the measured parameters (a) irradiance, (b) ambient temperature, (c) wind velocity and (d) PV cell temperature.

irradiance or nighttime [4]. Fig. 1(d) shows the Weibull distribution of the measured wind velocity. It is observed that the most frequent values are in the range of 3–5 m/s, with an average of 3.74 m/s and a standard deviation of 1.91 m/s. Values close to 1 m/s have a lower probability, while the maximum value was 12.5 m/s.

2.3. Local search: a simple and effective metaheuristic algorithm

Local search is a metaheuristic algorithm that focuses on finding high-quality solutions in a nearby search space. Unlike global algorithms that explore the entire solution space, local search aims to improve an initial solution through local changes. This approach is based on the idea that small modifications to a solution can lead to significant improvements [57]. The search process begins with an initial solution, and iterative local changes are made to search for neighboring solutions that are better in terms of a specific objective function. If a better solution is found, it becomes the new current solution, and the process continues. However, if no better solution is found, the algorithm may become trapped in a local optimum [43,58].

This metaheuristic algorithm is particularly useful for complex problems where full exploration of the search space is inefficient due to its large size. Local search has been successfully applied in several areas, including scheduling, resource allocation, network design, and route optimization, among others [59,60]. Its low computational cost, ease of use, and explainability [61] make the local search a suitable choice as the foundational algorithm for the present temperature computation problem.

2.4. The proposed metaheuristics-based method

The proposed metaheuristics-based method consists of a series of steps to calculate the nominal operating temperature of the PV module. A crucial aspect of the method is the use of the local search metaheuristic algorithm, which was briefly described in Section 2.3. A graphical explanation of the metaheuristics-based method is illustrated by an activity diagram in Fig. 2.

The proposed method is simple, and its simplicity is the main novelty. A critical component involves performing a proper data analysis (step 1) using the dataset (28304 × 3) taken from the DSM-270 PV module, followed by data preprocessing (step 2) and data normalization (step 3), to filter out irrelevant data and erroneous measurements, as explained in Section 2.2. This step 3, data normalization, not only provides a preprocessed data set, but also extracts basic parameters, such as the range of variables G_{NOCT} and $T_{a,NOCT}$, the mutation operators to move from the current point to the neighbors, and most importantly, how to evaluate the results of each iteration. Section 2.5 provides an explanation of this process. Additionally, an important step is the split of the dataset (step 4) into training data and validation data. Although it is not a classification task or other machine learning techniques, it is always essential to separate data to avoid biased results [62].

The step of applying restart local search (step 5) is explained in Section 2.5. It has its stopping condition, as outlined in pseudocode Algorithm 1; this step yields pairs of G_{NOCT} and $T_{a,NOCT}$. The pairwise sets are then used to perform the error analysis (step 6), based on the mean absolute error (MAE), so the validation set obtained in (step 4) is used. Pairwise sets of G_{NOCT} and $T_{a,NOCT}$ are substituted in the NOCT model described by Eq. (8) to calculate the estimated value of T_c. Then the error MAE between the estimated and measured values of T_c is analyzed. Eq. (4) explains MAE, presented in Section 2.7. Based on the study conducted by [56] at the National Renewable Energy Laboratory in the United States, successful results are considered when the condition $MAE < 3$ is reached. If $MAE > 3$, the process returns to (5), otherwise, the final values of G_{NOCT} and $T_{a,NOCT}$ are obtained.

2.5. Restart local search: Cuban data

After preprocessing and normalizing the dataset (step 2 and step 3), a set of clean data was obtained, as explained in Section 2.2. Fig. 1 shows the resulting values for irradiance and ambient temperature. This analysis helped to determine the input parameters for the restart local search algorithm, as described in Section 2.5.1. The pseudocode for our restart local search algorithm is presented in Section 2.6.

2.5.1. Input parameters for restart local search

Ranges of G_{NOCT} and $T_{a,NOCT}$; after analyzing the measured data (Fig. 1), the value of NOCT it set to 45 °C and the initial random solution should adhere to the following ranges:

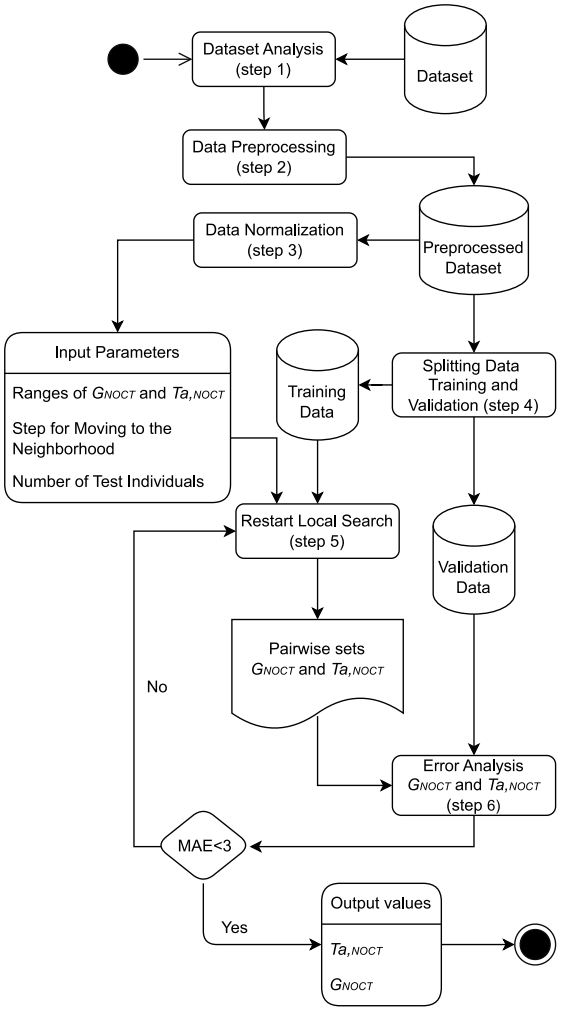

Fig. 2. Metaheuristics-based method for exploring numerous potential states of the parameters G_{NOCT} and $T_{a,NOCT}$ in the NOCT model under site-specific meteorological conditions.

- Ambient temperature: $T_{a,NOCT}$ = 25–35 °C; are the values with the highest probability.
- Irradiance: G_{NOCT} = 700–900 W/m^2; the third peaks registered are closest to the STC and NOCT conditions.

Neighborhood Steps: In local search, a mutation operator is a function or procedure used to modify the current solution and generate a neighboring solution within the search space. The purpose of this operator is to explore the search space for potentially better solutions. The mutation operator applies random changes to the current solution, which may include swapping, inversion, insertion, or any other relevant changes specific to the problem. These changes allow the exploration of different neighborhoods around the current solution in search of potential improvements. The choice and design of the mutation operator depends on the specific context in which the local search algorithm is applied [60]. An effective mutation operator should strike a balance between exploring the search space to avoid getting trapped in local optima and exploiting the best solutions found so far.

In this case, the mutation operator for both variables was defined as: increase, decrease, or keep the value of $G_{NOCT}current$ and $T_{a,NOCT}current$, respectively. The increment or decrement step size was 0.1 °C and 1 W/m^2 for $T_{a,NOCT}current$ and $G_{NOCT}current$, respectively. The possible combinations of the mutation operator are shown in the Table 3.

Table 3
Possible combinations of the mutation operator.

Parameters	Mutation combination							
$T_{a,NOCT}$ *current* (°C)	+0.1	+0.1	+0.1	−0.1	−0.1	−0.1	+0	+0
G_{NOCT} *current* (W/m^2)	+1	−1	+0	−1	+1	+0	−1	+1

The steps for making these decisions are explicitly detailed below and are based on the analysis of the available data. For $T_{a,NOCT}$, the step size to move in the search space is 0.1 °C in the movement range defined in Table 3. Dividing the unit into 10 parts allows for the possibility of having 100 possible neighbors, allowing for a less abrupt transition from the current state to a neighboring state. Similarly, for G_{NOCT}, the step size for movement is 1 W/m^2 in the range of movement defined in Table 3, resulting in 200 possible states for this variable. This gives a total of 20000 possible combinations to explore the neighborhood.

Number of validation individuals: for conducting the validations in each iteration, 5 individuals were selected. The selection of this number was determined through a Design of Experiment that involved 5, 10, 15, and 20 individuals [63]. The optimal population size was found to be 5 individuals per iteration. These individuals are randomly chosen from the entire training dataset.

The objective function used in the restart local search described in line 12 of the Algorithm 1, is an instance of MAE error described in Eq. (4). It is referred to as an instance of MAE because it is calculated using $G_{NOCT}current$ and $T_{a,NOCT}current$ of the current iteration, and only the quantity of validation individuals chosen in that iteration is used.

2.6. Restart local search: pseudocode

All input parameters explained in Section 2.5.1 were taken into account to run the algorithm. In addition, the following parameters were set $max\_iterations$ = 1000, $repetitions$ = 20 and $restarts$ = 300. During each iteration, all eight possible mutations are performed, and the one that produces the best results is selected as the new current value. The pseudocode used for the proposed method, along with the analyzed Cuban data, is shown in Algorithm 1.

2.7. Validation of the proposed method

The proposed algorithm was executed using datasets from the DSM-270 PV module, which comprises a data matrix of size 28304 × 3. In the model obtained, T_c was calculated using a dataset from the JKM265PP PV module, which comprises a matrix of size 39069 × 3. The validation was facilitated by four statistical metrics: MAE, mean absolute percentage error ($MAPE$), root mean square error ($RMSE$) and coefficient of determination (R^2), represented by Eqs. (4), (5), (6), and (7), respectively.

$$MAE = \frac{1}{n}\sum_{i=1}^{n}\left|T_{c,m} - T_{c,e}\right| \tag{4}$$

$$MAPE = \frac{1}{n}\sum_{i=1}^{n}\left|\frac{T_{c,m} - T_{c,e}}{T_{c,m}}\right| 100\% \tag{5}$$

$$RMSE = \sqrt{\frac{1}{n}\sum_{i=1}^{n}(T_{c,m} - T_{c,e})^2} \tag{6}$$

$$R^2 = 1 - \frac{\sum_{i=1}^{n}(T_{c,m} - T_{c,e})^2}{\sum_{i=1}^{n}(T_{c,m} - \overline{T_{c,m}})^2} \tag{7}$$

The indices (m) and (e) represent the measured and estimated values, respectively, n represents the number of data points and $\overline{T_{c,m}}$ represents the average of the measured values.

Algorithm 1 Restart local search: pseudocode.

Require: *parameter*: Parameter list
Ensure: G_{NOCT} and $T_{a,NOCT}$
x= G_{NOCT}*current*
y= $T_{a,NOCT}$*current*
Function *load_data*()
Open the CSV file *datatrain.csv* in read mode
Initialize an empty list called *readings*
for each row in the CSV file **do**
    Split the row by the delimiter ; and add it to the *readings* list
end for
Close the CSV file
Return *readings*
Function *objective_function*(x,y,G,T_a,T_c):
Return the absolute value of $(T_c - (T_a + G/x * (45 - y)))$
Function *mutate*():
Initialize the list *possibilities* with the combinations in Table 3
Return a randomly selected combination from the list *possibilities*
Function *guided_scaling* (*max_iterations*, *step_size_x*, *step_size_y*, *sample_size*, *restarts*, *range_x*, *range_y*):
readings = load_data()
Initialize an empty list called *history*
Initialize *best_solution* as None
Initialize *best_score as* $+\infty$
Initialize x and y as random values based on *range_x* and *range_y*
for Each iteration in the range *max_iterations* **do**
    Generate a random sample of size *sample_size* by selecting random rows from *readings*
    Initialize an empty list called *differences*
    for Each sample in the samples **do**
        Get the values G, T_a, and T_c from the sample
        Calculate the difference using the *objective_function* and add it to *differences*
    end for
    Calculate the *current_score* as the sum of *differences* divided by it is length
    Add [x, y, *current_score*] to *history*
    if The *current_score* is better than *best_score* **then**
        Update *best_score* with the *current_score*
    else
        Keep *best_score*
    end if
    Generate all possible mutations and store them in the *mutations* list
    Adjust the values in *mutations* based on *range_x* and *range_y*
    Initialize an empty list called *neighbor_scores*
    for Each mutation in *mutations* **do**
        Calculate the coordinates of the neighbor by adding the *step_size_x* and *step_size_y* to x and y
        Initialize an empty list called *temp_scores*
        for Each sample in the samples **do**
            Get the values G, T_a, and T_c from the sample
            Calculate the score using the objective function and add it to *temp_scores*
        end for
        Calculate the average from *temp_scores* and add it to *neighbor_scores* with the coordinates of the neighbor
    end for
    Get the neighbor with the lowest score from *neighbor_scores*
    Update x and y with the coordinates of the neighbor
end for

3. Results and discussions

After applying the method (Fig. 2) using the DSM-270 PV module dataset, pairwise G_{NOCT} and $T_{a,NOCT}$ were obtained which best corresponded to the model (8) for the Cuban scenario.

Table 4
Ranking according to the MAE metric of evaluated thermal models (4–22) and the proposed model (8) applied to DSM-270 PV module.

Ranking	Model	MAE (°C)	$MAPE$ (%)	$RMSE$ (°C)	R^2
1	(8)	2.34	6.60	2.57	0.74
2	(20)	2.55	7.23	2.70	0.73
3	(15)	3.07	8.86	4.33	0.59
4	(17)	3.18	9.18	4.44	0.59
5	(19)	3.55	10.34	4.01	0.66
6	(21)	3.67	10.41	4.16	0.68
7	(9)	4.80	13.52	3.67	0.72
8	(18)	5.58	15.77	3.95	0.72
9	(11)	5.74	16.20	3.78	0.74
10	(13)	6.20	17.45	3.93	0.73
11	(22)	6.80	19.07	4.13	0.72
12	(12)	7.19	19.99	5.37	0.65
13	(14)	7.98	22.28	4.56	0.71
14	(10)	7.99	22.30	4.54	0.72
15	(5)	8.53	23.77	5.16	0.66
16	(7)	8.83	24.38	5.60	0.65
17	(4)	10.82	29.97	5.99	0.65
18	(16)	11.36	31.43	6.18	0.64
19	(8)	11.49	31.79	6.23	0.64
20	(6)	16.61	46.89	5.48	0.69

Table 5
Ranking according to the MAE metric of evaluated thermal models (4–22) and the proposed model (8) applied to JKM265PP PV module.

Ranking	Model	MAE (°C)	$MAPE$ (%)	$RMSE$ (°C)	R^2
1	(20)	2.89	7.00	2.58	0.76
2	(8)	3.14	7.54	2.45	0.77
3	(9)	3.17	8.19	3.52	0.74
4	(21)	3.33	8.63	4.32	0.67
5	(15)	3.71	9.44	4.63	0.52
6	(17)	3.71	9.46	4.75	0.52
7	(11)	4.15	10.83	4.16	0.70
8	(18)	4.16	10.89	4.42	0.67
9	(13)	4.51	11.69	4.21	0.71
10	(22)	4.97	12.84	4.36	0.71
11	(19)	5.07	12.93	4.18	0.64
12	(12)	5.84	14.95	5.57	0.64
13	(14)	6.13	15.68	4.80	0.70
14	(10)	6.21	15.89	4.87	0.70
15	(5)	6.34	16.13	5.01	0.69
16	(7)	6.76	16.95	5.47	0.69
17	(4)	8.59	21.64	5.86	0.68
18	(16)	9.12	22.94	6.05	0.68
19	(8)	9.25	23.26	6.10	0.68
20	(6)	14.72	38.24	5.69	0.67

3.1. Proposed model according to Cuban data

In step 5 of the method, a total of 28 pairwise sets G_{NOCT} and $T_{a,NOCT}$ were obtained, varying within the ranges 702.92–894.83 W/m^2 and 25.32–34.90 °C, respectively. The algorithm followed the limits defined in Section 2.5.1. The pairwise set obtained by the metaheuristic method iterations are shown in Fig. 3, the results complied with $MAE < 3$ error are marked in gray. The execution time for each run of the algorithm was ranged 5–20 s.

The 28th iteration yielded the lowest MAE. The values of G_{NOCT} and $T_{a,NOCT}$ corresponding to this iteration are represented by Eq. (8) and demonstrate the strongest correlation found for the tropical climatic conditions of Cuba.

$$T_c = T_a + \frac{G}{869.63}(NOCT - 34.90) \tag{8}$$

Based on the model (8) of Table 1, the parameters G_{NOCT} and $T_{a,NOCT}$ were recomputed, obtaining the new values $G_{NOCT} = 869.63 \pm 1$ W/m^2 and $T_{a,NOCT} = 34.90 \pm 0.1$ °C for the wind velocity of 3–5 m/s. Both parameters resulted in values higher than the NOCT conditions

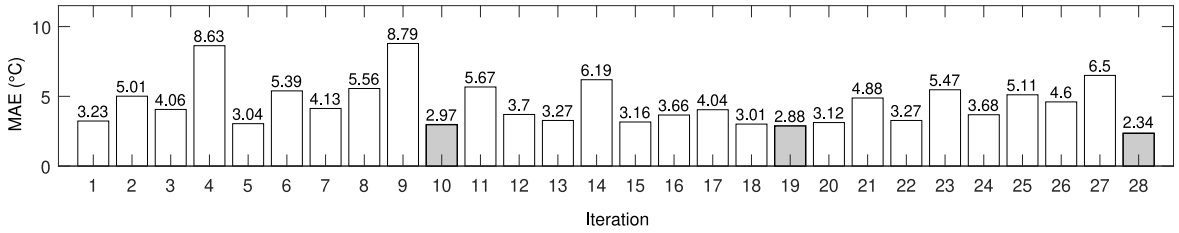

Fig. 3. Mean absolute error (MAE) versus number of iterations obtained through the application of the proposed local search-based method.

recommended by IEC Standard 61215-1, resulting in a lower nominal operating temperature. Therefore, the applied methodology shows that the average values of irradiance and ambient temperature during peak solar hours are the best climatic conditions to estimate the nominal operating temperature.

3.2. Evaluation of the models

The algorithm was executed using a dataset from DSM-270 PV module, while to evaluate the model obtained in Eq. (8), a separate dataset from JKM265PP PV module was used, as explained in Section 2.7. In this section, both dataset are used to evaluate the accuracy of the models shown in Table 1.

For easily understanding, in this study the model is referred by the equation number, e.g., the evaluated thermal models correspond to (4–22), while model (8) is the proposed thermal model. Based on the datasets, comparative assessments of model (8) with each model listed in Table 1 were performed. Fig. 4 shows the metrics defined by Eqs. (4)–(7). Tables 4 and 5 show the ranking according to the MAE metric for the DSM-270 and JKM265PP PV modules, respectively.

Tables 4 and 5 show model (8) ranked in 1st and 2nd position (highlighted in gray). It is observed that the positions ranked from 1st to 7th were models that calculated T_c with high accuracy. Although the position in Table 4 is different from the positions in Table 5, the models (8), (20), (15), (17), (19), (21) and (9) determine the operating temperature more accurately for the Cuba data. Models (15), (17), (19) and (21) use wind velocity as an input parameter, which improves the prediction of T_c. Conversely, the positions ranked from 8th to 20th are occupied by almost the same models between Tables 4 and 5. Due to the similarity of the physical properties of both PV modules (see Table 2), these similar results are consistent in both tables. Model (8) (highlighted in green) recommended by IEC Standard 61215-1, was ranked in the 19th position for both modules, because it is effective in the limited meteorological conditions described in Section 2.2.

Model (20) established by [14] ranks 2nd in the Table 4 and 1st in Table 5, this research was also conducted under tropical climate conditions (Malaysian study with input parameters $G_{tFOCT} = 886$ W/m^2 and $T_{a,tFOCT} = 34$ °C). This result confirms the assumption that PV installations operating in this type of climate need to fix the parameters of the model (8).

After evaluating the results of the DSM-270 PV module shown in Table 4, models (8) and (20) were the highest-ranked models according to the metrics. Conversely, the analysis of the MAE and $MAPE$ metrics showed that models (8) and (6) were the worst performing. The $RMSE$ metric showed that model (8) had the poorest value with $RMSE = 6.23$ °C while models (8) and (11) had the highest score for the R^2 metric, with ($R^2 = 0.74$ for both models). In each instance, results for models (15) and (17) were the worst, with $R^2 = 0.59$.

By analyzing the results of the JKM265PP PV module shown in Table 5, models (20) and (8) are the highest-ranked. For MAE and $MAPE$ metrics, models (8) and (6) presented the worst value. According to the $RMSE$ metric, model (8) presented the worst value $RMSE = 6.10$ °C. Based on the R^2 metric, models (8) and (20) demonstrated best values, conversely models (15) and (17) presented the worst values ($R^2 = 0.52$ in each case).

The metric R^2 is explained graphically in Fig. 5, which shows the linear fit plot of G and T_a with T_c, of the evaluated thermal models (4–22) and the proposed model (8). The models vary linearly with both T_a and G with different slopes. The analysis suggests that the models predict T_c differently when exposed to the same operating conditions. For example, model (19) underestimates T_c for $G < 1200$ W/m^2 (Fig. 5(a)) and $T_a < 35$ °C (Fig. 5(b)); while the rest of the models have an overestimation behavior.

In Fig. 5(a), for the conditions $G_{NOCT} = 869.63$ W/m^2, the models (15) and (17) presented low operating temperatures in the range of $T_c = 40$–50 °C. Models (20) and (8) were the best performers, with slight variations in the measured temperature range $T_c = 40$–45 °C. On the opposite, model (6) presented highest operating temperatures of $T_c = 60$–70 °C, and for the maximum values of irradiance measured ($G = 1199.60$ W/m^2) it is even in the range of $T_c = 70$–80 °C. Based on the cell temperature measurements shown in Fig. 1(c), models (4), (5), (6), (7), (8), (10), (12), (14) and (16) overestimate the maximum value of $T_c = 57.10$ °C.

In Fig. 5(b), for the conditions $T_{a,NOCT} = 34.90$ °C, the models (15), (17), (19), (20), and (21) presented low operating temperatures in the range of $T_c = 40$–50 °C, therefore, correctly calculating the cell temperature, due to the incorporation of v_w as input parameter; on the opposite, models (4), (6), (8) and (16) presented the highest temperatures, in the order of $T_c \geq 60$ °C, which is the worst correlation of T_c with input parameter T_a.

Based on the findings presented in Table 4, Table 5 and Fig. 5, it can be concluded that the proposed thermal model establishes a stronger correlation between the meteorological factors of Cuba and cell temperature. By contrast, the NOCT model (model (8)) presented the worst performance. In Table 4, model (8) decreased the MAE, MAPE and RMSE of model (8) by 4.91, 4.82 and 2.42 times, respectively. In Table 5, model (8) reduced the MAE, MAPE and RMSE of model (8) by 2.95, 3.08 and 2.49 times, respectively.

3.3. Comparison of the predictive capacity for daily profiles

To assess the performance of the models for daily profiles, a comparative analysis of specific days has been conducted. Fig. 6 shows three days chosen because the input parameters of the evaluated thermal models (G, T_a and v_w) had a varied behavior. Fig. 6(a) shows a partly cloudy day with irregular irradiance (July 5, 2021), Fig. 6(c) shows a sunny day with regular irradiance (August 29, 2021) and Fig. 6(e) shows a cloudy day with low irradiance (November 4, 2021). The months of July and August in which T_a are greater at the summer period, despite the eventual irregularity of the incident irradiance, and the month of November, with a low level of G and T_a have been selected. Figs. 6(b), 6(d), 6(f) depicts T_c values determined using the evaluated thermal models, applied to the DSM-270 PV module for each day. Table 6 shows the ranking of the models, according to the metrics of Eqs. (4)–(7), for the three different meteorological scenarios shown in Figs. 6(a), 6(c), 6(e).

On July 5, 2021, represented in Fig. 6(a), an irradiation of 5.39 kWh/m^2 was registered, in accordance to the average daily value for Cuba of 5 kWh/m^2 [51]. The maximum irradiance value G =

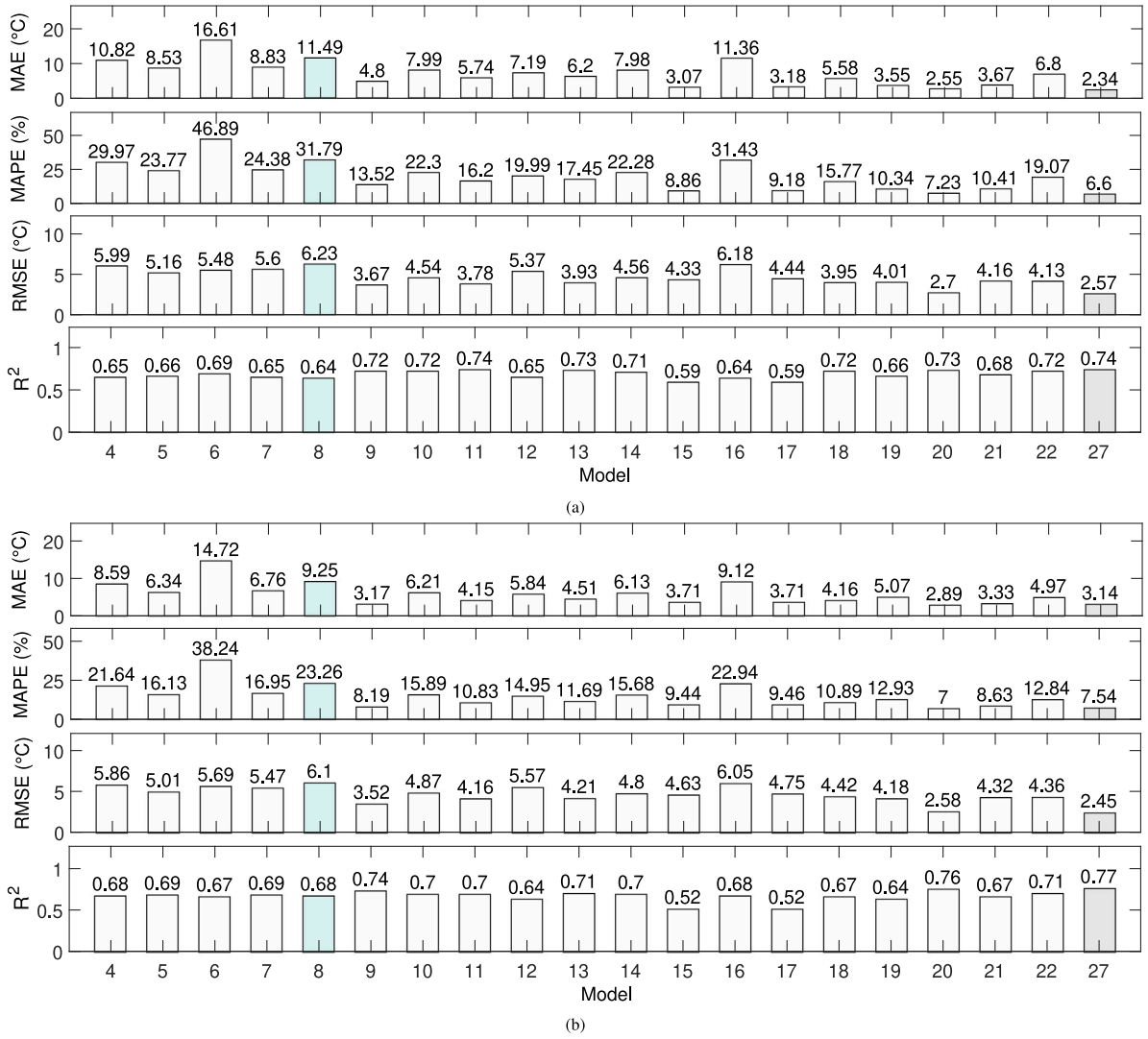

Fig. 4. Metrics for the comparison of evaluated thermal models (4–22) and the proposed model (8) applied to (a) DSM-270 and (b) JKM265PP PV modules.

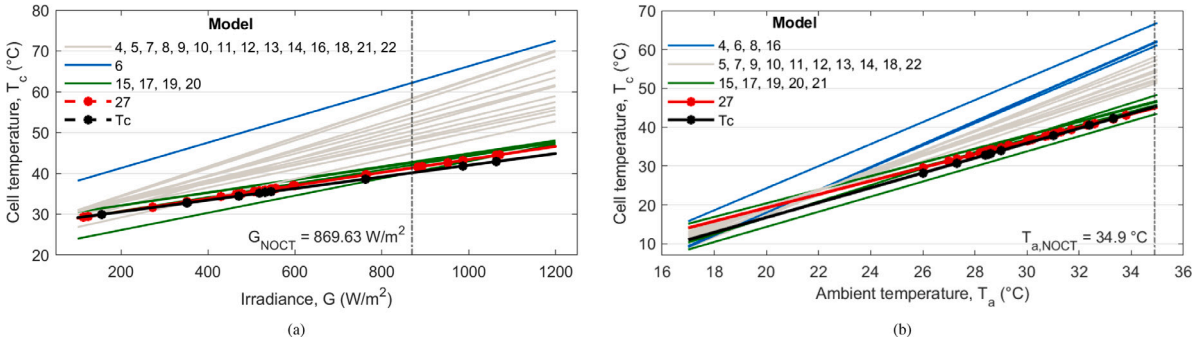

Fig. 5. Linear fit plot of (a) T_c vs G and (b) T_c vs T_a, for the evaluated thermal models (4–22) and the proposed model (8) applied to DSM-270 PV module.

1091.90 W/m^2 was registered at 13:00 h and the maximum cell temperature T_c = 52.60 °C was registered at 13:10 h. The ambient and cell temperature values were in the ranges T_a = 23.20–36.70 °C and T_c = 21.90–52.60 °C, respectively; the average wind velocity was v_w = 1.80 m/s with a standard deviation of 1.87 m/s. According to the findings shown in Table 6 and Fig. 6(b), model (6) was the less accurate, overestimating the maximum cell temperature, with T_c = 32.15–80.72 °C and the metrics MAE = 14.27 °C, $MAPE$ = 47.56%, $RMSE$ = 4.48 °C and R^2 = 0.85. Model (8) was the most accurate, reaching the values of cell temperature in the range T_c = 23.20–48.25 °C, with metrics MAE = 1.88 °C, $MAPE$ = 6.12%, $RMSE$ = 1.99 °C and R^2 = 0.92. The analysis of the maximum measured and predicted cell temperatures values, showed models (8) and (6) have an MAE = −4.35 °C (underestimation) and MAE = +28.12 °C (overestimation),

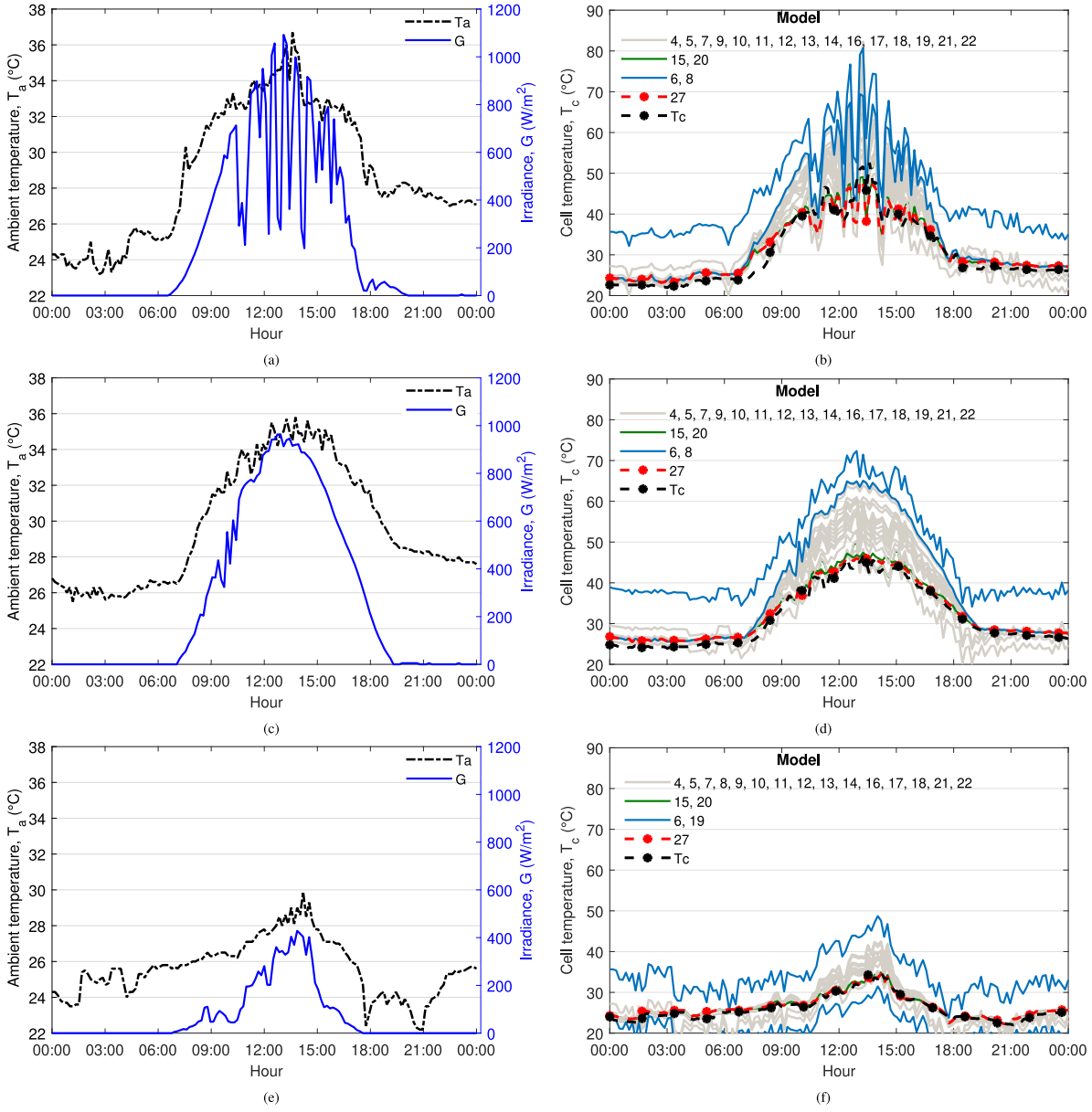

Fig. 6. Measurements of irradiance and ambient temperature on (a) July 5, 2021, a partly cloudy day with irregular and high level of irradiance, (c) August 29, 2021, a clearsky day with regular irradiance and (e) November 4, 2021, a cloudy day with low level of irradiance; (b, d, f) the cell temperature predicted by the evaluated thermal models (4–22) and the proposed model (8), applied to DSM-270 PV module.

respectively. It can be concluded that the difference in the maximum temperature values reached by the models is significant.

On August 29, 2021, represented in Fig. 6(c), a high level irradiation of 6.48 kWh/m^2 was registered, above the average daily for Cuba. The maximum irradiance value $G = 963.40$ W/m^2 was observed at 12:20 h and the maximum cell temperature $T_c = 46.60$ °C at 12:50 h. The ambient and cell temperature values were in the range of $T_a = 25.50$–35.80 °C and $T_c = 23.80$–46.60 °C, respectively; the average wind velocity was $\upsilon_w = 2.46$ m/s with a standard deviation of 1.90 m/s. The results presented in Table 6 and Fig. 6(d) show the models (8) and (6) were less accurate, overestimating the cell temperature. In the case of model (6), predicted values were in the range of $T_c = 34.14$–72.34 °C, with the metrics $MAE = 14.61$ °C, $MAPE = 45.85\%$, $RMSE = 3.08$ °C and $R^2 = 0.93$. Models (8), (20) and (15) were the most accurate; model (8) predicted values were in the range $T_c = 25.50$–46.61 °C, with the metrics $MAE = 1.22$ °C, $MAPE = 4.15\%$, $RMSE = 0.66$ °C and $R^2 = 0.99$. In analysis of the maximum measured and predicted cell temperature values, models (8) and (6) have an $MAE = -0.01$ °C (underestimation) and $MAE = +25.77$ °C (overestimation), respectively. In this instance, model (8) largely reduced the difference between maximum measured and the predicted cell temperature.

On November 4, 2021, represented in Fig. 6(e), a low level irradiation of 1.63 kWh/m^2 was registered, due to cloudiness and low intensity of the irradiance. It was registered the maximum irradiance value $G = 428.40$ W/m^2 at 13:40 h and the maximum cell temperature $T_c = 35.00$ °C at 14:00 h. The ambient and cell temperature values were in the range of $T_a = 22.20$–29.90 °C and $T_c = 22.00$–35.00 °C, respectively. This day presented meteorological conditions where the wind velocity was higher than other days analyzed, the average wind velocity was $\upsilon_w = 3.19$ m/s with a standard deviation of 1.51 m/s. According to the findings shown in Table 6 and Fig. 6(f), models (19) and (6) were the least accurate; in the case of model (6), values of $T_c = 23.75$–48.73 °C and metrics $MAE = 8.10$ °C, $MAPE = 31.09\%$, $RMSE = 2.67$ °C and $R^2 = 0.72$. Models (8), (20) and (15) were the most accurate; in

Table 6
Metrics for the comparison of evaluated thermal models (4–22) and the proposed model (8) for the selected days, applied to DSM-270 PV module.

Date	Ranking	Model	Metric				Predicted cell temperature		
			MAE (°C)	$MAPE$ (%)	$RMSE$ (°C)	R^2	Minimum (°C)	Average (°C)	Maximum (°C)
July 5, 2021	1	(8)	1.88	6.12	1.99	0.92	23.20	31.45	48.25
	2	(20)	1.93	6.26	2.09	0.92	23.20	31.63	49.10
	3	(15)	2.55	7.92	3.80	0.83	23.20	32.46	81.17
	4	(17)	2.60	8.05	3.89	0.82	23.20	32.55	82.26
	5	(19)	2.74	8.35	3.33	0.82	20.05	29.17	54.87
	6	(9)	2.77	8.37	2.82	0.91	22.70	33.06	55.75
	7	(21)	2.80	8.99	3.40	0.85	22.42	31.91	58.77
	8	(11)	3.33	9.93	3.40	0.89	23.20	33.71	68.91
	9	(18)	3.35	9.98	3.63	0.88	23.20	33.73	73.88
	10	(13)	3.46	10.25	3.38	0.90	23.20	33.85	66.00
	11	(22)	3.67	10.79	3.51	0.89	23.20	34.09	67.03
	12	(7)	3.76	10.12	4.24	0.88	22.20	34.12	64.87
	13	(14)	4.12	11.92	3.81	0.89	23.20	34.60	68.82
	14	(5)	4.16	12.03	3.91	0.88	23.20	34.61	63.36
	15	(10)	4.17	12.04	3.88	0.89	23.20	34.66	70.77
	16	(12)	4.83	15.46	4.37	0.82	24.00	35.02	67.78
	17	(4)	5.03	14.23	4.53	0.88	23.20	35.57	68.06
	18	(16)	5.24	14.75	4.67	0.87	23.20	35.80	69.15
	19	(8)	5.29	14.88	4.71	0.87	23.20	35.85	69.42
	20	(6)	14.27	47.56	4.48	0.85	32.15	44.94	80.72
August 29, 2021	1	(8)	1.22	4.15	0.66	0.99	25.50	32.88	46.61
	2	(20)	1.42	4.65	0.71	0.99	25.50	33.09	47.36
	3	(15)	1.50	4.89	1.32	0.97	25.50	32.99	49.95
	4	(17)	1.54	5.01	1.35	0.97	25.50	33.07	50.32
	5	(21)	2.24	6.79	2.34	0.93	23.73	32.93	52.50
	6	(19)	2.37	7.62	2.53	0.90	20.21	29.90	48.03
	7	(18)	3.17	9.02	1.60	0.97	25.50	34.88	56.69
	8	(9)	3.18	9.01	1.02	0.99	25.33	34.89	53.39
	9	(11)	3.35	9.45	1.47	0.98	25.50	35.06	56.59
	10	(13)	3.68	10.27	1.49	0.98	25.50	35.39	57.39
	11	(22)	3.99	11.01	1.50	0.98	25.50	35.70	58.17
	12	(10)	4.59	12.52	1.76	0.98	25.50	36.30	61.01
	13	(14)	4.62	12.57	1.67	0.98	25.50	36.33	60.52
	14	(7)	4.65	11.86	1.78	0.98	24.50	36.30	61.00
	15	(12)	4.80	14.10	3.05	0.92	24.53	36.14	60.14
	16	(5)	4.97	13.40	1.62	0.98	25.50	36.68	59.84
	17	(4)	6.13	16.27	1.93	0.98	25.50	37.84	63.88
	18	(16)	6.40	16.94	2.00	0.98	25.50	38.11	64.82
	19	(8)	6.47	17.10	2.02	0.98	25.50	38.18	65.06
	20	(6)	14.61	45.85	3.08	0.93	34.14	46.32	72.34
November 4, 2021	1	(8)	0.56	2.22	0.45	0.97	22.20	26.42	34.58
	2	(20)	0.59	2.32	0.46	0.97	22.20	26.48	34.91
	3	(15)	0.62	2.44	0.51	0.97	22.20	26.49	35.12
	4	(17)	0.63	2.47	0.52	0.97	22.20	26.51	35.28
	5	(9)	0.83	3.03	0.58	0.98	21.56	26.67	37.40
	6	(18)	1.05	3.84	0.64	0.97	22.20	26.97	38.04
	7	(11)	1.08	3.96	0.64	0.97	22.20	27.01	38.00
	8	(7)	1.15	4.03	0.86	0.97	21.20	26.54	40.19
	9	(13)	1.17	4.25	0.67	0.97	22.20	27.10	38.34
	10	(22)	1.24	4.47	0.70	0.97	22.20	27.17	38.77
	11	(10)	1.41	5.02	0.78	0.97	22.20	27.33	39.91
	12	(14)	1.41	5.01	0.77	0.97	22.20	27.33	39.74
	13	(5)	1.46	5.18	0.79	0.97	22.20	27.38	40.26
	14	(4)	1.75	6.14	0.93	0.96	22.20	27.68	42.00
	15	(16)	1.82	6.37	0.96	0.96	22.20	27.75	42.40
	16	(8)	1.84	6.42	0.97	0.96	22.20	27.76	42.50
	17	(12)	2.15	8.36	2.53	0.69	16.71	25.51	38.96
	18	(21)	2.41	9.50	2.01	0.72	16.18	23.81	34.83
	19	(19)	4.98	19.30	2.38	0.59	12.77	20.99	31.47
	20	(6)	8.10	31.09	2.67	0.72	23.75	34.05	48.73

the case of model (8), reaching the values T_c = 22.20–34.58 °C, with the metrics MAE = 0.56 °C, $MAPE$ = 2.22%, $RMSE$ = 0.45 °C and R^2 = 0.97. Under these meteorological conditions, according to MAE, MAPE and RMSE metrics; the proposed thermal model (8) performed better compared to the other analyzed days. Similar to the other days, models (8) and (8) had an error MAE = −0.42 °C (underestimation) and MAE = +7.50 °C (overestimation), between maximum measured and the predicted cell temperature.

The results illustrated in Fig. 6 and Table 6 allow the assertion that model (8) has a robust correlation between T_c and G, T_a under different climate scenarios, including a clear sky day with high irradiance and a cloudy day with low irradiance. The evaluation of short- and long-term performance metrics demonstrated the necessity to compute the cell temperature using the appropriate approach for the specific meteorological conditions at the PV system site. Therefore, the generated power can be accurately predicted using model (8), for a high level of ambient temperature, such as on August 29, 2021. In the opposite, the

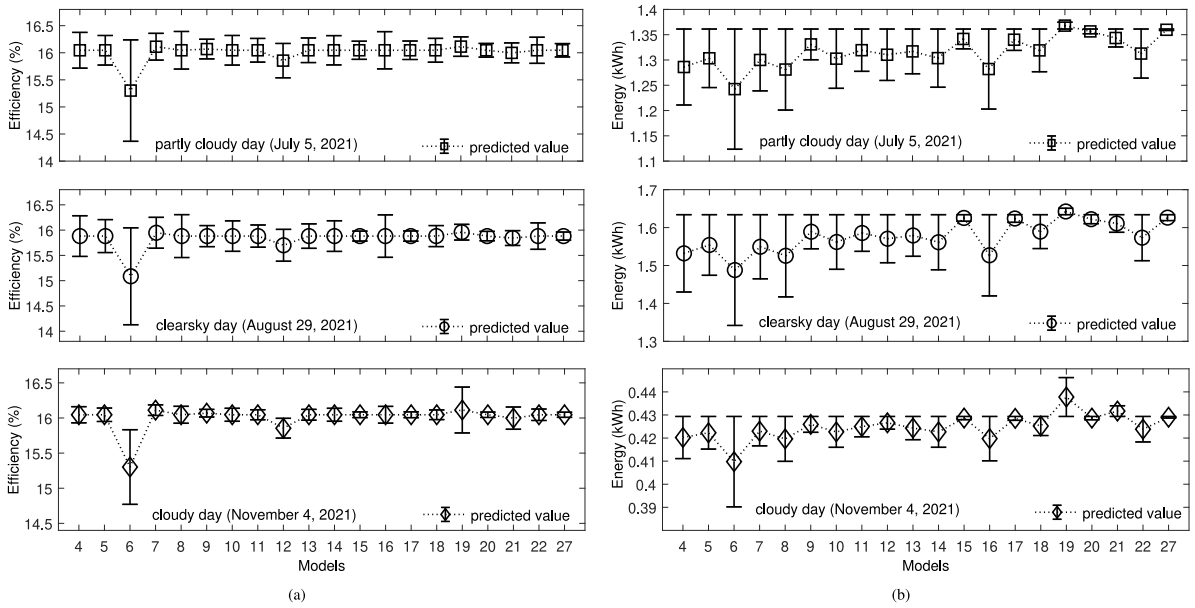

Fig. 7. Predictive capacity of the evaluated thermal models (4–22) and the proposed model (8) on (a) the efficiency and (b) the produced energy for the selected days, applied to the DSM-270 PV module and the installation; the errorbars show the MAE metric.

Table 7
Daily produced energy by the evaluated thermal models (4–22) and the proposed model (8) during the analyzed days.

Model	July 5, 2021			August 29, 2021			November 4, 2021		
	$E_{c,day}$ (kWh)	$E_{i,day}$ (kWh)	$MAPE_i$ (%)	$E_{c,day}$ (kWh)	$E_{i,day}$ (kWh)	$MAPE_i$ (%)	$E_{c,day}$ (kWh)	$E_{i,day}$ (kWh)	$MAPE_i$ (%)
(4)	1.286	11.317	5.518	1.532	13.482	6.240	0.420	3.698	2.125
(5)	1.303	11.469	4.251	1.554	13.676	4.890	0.422	3.716	1.646
(6)	1.242	10.932	8.732	1.487	13.094	8.937	0.409	3.606	4.561
(7)	1.300	11.440	4.491	1.549	13.635	5.174	0.422	3.722	1.483
(8)	1.281	11.273	5.886	1.525	13.425	6.632	0.419	3.692	2.264
(9)	1.330	11.711	2.233	1.589	13.983	2.751	0.425	3.748	0.799
(10)	1.302	11.462	4.306	1.562	13.745	4.407	0.422	3.719	1.556
(11)	1.319	11.610	3.073	1.585	13.954	2.957	0.424	3.739	1.025
(12)	1.310	11.531	3.735	1.570	13.821	3.878	0.426	3.754	0.642
(13)	1.316	11.589	3.250	1.579	13.896	3.357	0.424	3.734	1.172
(14)	1.303	11.472	4.227	1.561	13.740	4.445	0.422	3.719	1.554
(15)	1.341	11.806	1.438	1.625	14.303	0.527	0.428	3.772	0.162
(16)	1.282	11.282	5.813	1.526	13.437	6.553	0.419	3.693	2.237
(17)	1.340	11.792	1.553	1.623	14.290	0.616	0.428	3.770	0.196
(18)	1.318	11.606	3.103	1.589	13.986	2.733	0.425	3.742	0.962
(19)	1.367	12.038	0.496	1.642	14.454	0.518	0.437	3.852	1.961
(20)	1.356	11.937	0.343	1.622	14.274	0.727	0.428	3.772	0.167
(21)	1.343	11.822	1.302	1.610	14.175	1.420	0.431	3.798	0.539
(22)	1.312	11.551	3.564	1.573	13.845	3.712	0.423	3.729	1.285
(8)	1.359	11.965	0.107	1.626	14.311	0.476	0.429	3.775	0.078

other models tended to overestimate the cell temperature, which results in underestimating the generated power.

Applying Eq. (3) with the measurements of cell temperature on the selected days, the daily produced energy was obtained: $E_{c,day}$ = 1.361 kWh, $E_{c,day}$ = 1.634 kWh and $E_{c,day}$ = 0.429 kWh on July 5, August 29 and November 4, 2021, respectively. The daily energy produced by the PV installation $E_{i,day}$, as per the specifications described in Section 2.1, is $E_{i,day}$ = 11.978 MWh, $E_{i,day}$ = 14.379 MWh and $E_{i,day}$ = 3.778 MWh, respectively, for the selected days. The amount of daily produced energy was significantly affected by irradiance under the different meteorological scenarios.

Fig. 7 and Table 7 depict the predictive ability on the efficiency and the produced energy for the selected three days, applying Eq. (1) and (3) to the thermal models (4) and (22) and the proposed thermal model (8). By analysis of the predictive capability of the efficiency shown in Fig. 7(a), models (19) and (8) have efficiency values above the other models, the latter tending to overestimate the cell temperature, and consequently, efficiency is underestimated. However, model (8) has the lowest error levels and shows the most accurate prediction, while models (6) and (8) were the least accurate, with wider error ranges, for the selected days. Fig. 7(b) shows a similar response to Fig. 7(a) for the predictive capability of the produced energy. Overall, under the meteorological conditions of November 4, 2021, the models predicted the efficiency and produced energy more accurately.

Through analysis of the results presented in Table 7, adjusting the values of G_{NOCT} and $T_{a,NOCT}$, the proposed thermal model (8) (highlighted in gray) significantly reduced the MAPE error of model (8) (highlighted in green) by 54.86, 13.93, and 28.85 times on July 5, August 29 and November 4, 2021, respectively. However, an inaccurate prediction of T_c resulted in an inaccurate prediction of PV conversion efficiency and therefore the amount of produced energy. It could also cause errors in the prediction of PV module lifetime. Indeed, as the T_c exceeds 45 °C, the degradation process is enhanced [64].

3.4. Final discussion

The adoption of a metaheuristic as the basis of the proposed method has proven to be highly efficient, producing excellent results without the need to perform an exhaustive search of all possible combinations. It improves the process and reduces and significantly reduces the execution time required to obtain G_{NOCT} and $T_{a,NOCT}$ and has minimized the MAE error, this is also due to the low algorithm complexity that the restart local search has. An innovative aspect of this study lies in the treatment of the data set, where the identification and elimination of erroneous values in the measurements allow to start the search from the best values in a more accurate and efficient way. This approach simplifies the process and improves the robustness and reliability of the results.

The estimated and measured cell temperature values were compared, considering a 23-month period, to obtain long-term model validation. Evaluation metrics demonstrated that the proposed thermal model (8) was ranked in 1st and 2nd positions for the DSM-270 and JKM265PP PV modules, respectively. Similarly, the three daily profiles in different months of the year were used to obtain short-term model validation. Under these meteorological conditions, the proposed thermal model (8) was ranked in 1st position for both PV modules. These findings demonstrate the accuracy of the local search-based algorithm applied to predict long- and short-term PV cell temperatures, improving the predictive capacity of the energy and efficiency of the PV systems studied.

Using the dataset of the currently operating PV systems in Cuba, the parameters G_{NOCT} and $T_{a,NOCT}$ of the NOCT model were adjusted from 800 W/m^2 to 869.63 W/m^2 and from 20 °C to 34.90 °C, respectively. To perform the adjustment of the parameters for Cuba, as outlined in the proposed method and described in Section 2.5, the data were divided into training and validation sets. The input data used in step 5 of the method presented in Fig. 2 was taken from the DSM-270 PV module dataset (training data). When the results were validated in step 6, using the dataset of the JKM265PP PV module (validation data), identical findings were obtained (Figs. 5, 6 and 7, as well as Tables 6 and 7).

The Cuban government aims to install 191 PV systems by 2030, to achieve a total installed capacity of 700 MW [50,51]. Therefore, based on the analyzed metrics and the fact that 63% of PV systems in Cuba have not been designed, sized, or installed, it is advisable to use thermal model (8) to enhance the forecasting accuracy of temperatures for PV modules, especially under these tropical climate conditions. Similar G_{NOCT} and $T_{a,NOCT}$ were computed for tropical environments (Malaysian case), resulting in an average absolute error of 1.72% [14]. The local search-based method shown in Fig. 2 and Algorithm 1 is suggested to compute the parameters G_{NOCT} and $T_{a,NOCT}$, in order to accurately predict the cell temperature under different meteorological conditions. Noteworthy, it is important to have a dataset of reliable measurements, at least one year of records. Also, including other input parameters, such as v_w and H_r, could enhance the accuracy of the results [32,33,37].

Given the similar electrical and mechanical characteristics of both PV modules (shown in Table 2), they reached the same cell temperature under the same conditions of ambient temperature and irradiance. DSM-270 multicrystalline silicon modules are manufactured in Cuba and are widely used in PV systems connected to the National Electroenergetic System. Multicrystalline silicon modules with similar characteristics were considered for this study. Different solar cell technologies have different responses to ambient temperature variations [65], it is then recommended to extend this study to monocrystalline or amorphous silicon technologies.

4. Conclusions

The wide range and variety of thermal models documented in the scientific literature, highlight the need to apply the most accurate model according to the specific location of the PV installation. To solve this identified issue, a local search-based method with restart was proposed to obtain the operating temperature of photovoltaic cells. The input parameters for the method consisted of meteorological variables recorded over a period of 23 months, including solar irradiance and ambient temperature. The main findings of this study were:

- The method is straightforward and pragmatic, as it analyzes the input values G_{NOCT} and $T_{a,NOCT}$. By using a restart local search, it has a low computational cost and also adheres to the principle of Explainable Artificial Intelligence.
- The NOCT model (8) recommended by IEC Standard 61215-1 is one of the less accurate among the 19 models analyzed. For the dataset over 23-month period, the proposed thermal model (8) reduced the MAE, MAPE and RMSE of model (8) by 4.91, 4.82 and 2.42 times, respectively.
- For three daily profiles with varying levels of irradiance, the proposed thermal model (8) yielded the lowest MAE error, obtaining 1.88 °C, 1.22 °C y 0.56 °C, respectively; consequently, enhanced it the prediction of the energy production and efficiency of the photovoltaic systems studied.
- Based on registered and preprocessed Cuban data, it is recommended to use the following values in the NOCT model to accurately calculate the operating cell temperature: G_{NOCT} = 869.63 W/m^2 and $T_{a,NOCT}$ = 34.90 °C, for a wind velocity of 4 ± 1 m/s.

The cell temperature directly affects the efficiency and produced energy. Therefore, to achieve the goal of installing a capacity of 700 MW by 2030 in Cuba, it is highly recommended to use the model (8) proposed in this paper for projects of designing and sizing PV systems. The findings are limited to multicrystalline silicon technology. While most PV modules installed in Cuba and future planned installations use this technology, it is imperative to create models that encompass all the PV varieties available on the market.

CRediT authorship contribution statement

Liomnis Osorio: Investigation, Software, Methodology, Visualization, Formal analysis, Writing – original draft, Writing – review & editing. **Mailyn Moreno:** Methodology, Resources, Data curation, Validation, Formal analysis, Writing – original draft, Writing – review & editing. **Marco Rivera:** Conceptualization, Supervision, Formal analysis, Writing – review & editing. **Víctor Tuninetti:** Conceptualization, Supervision, Formal analysis, Writing – review & editing. **Gerardo Ruíz Chavarria:** Data curation, Supervision, Validation, Formal analysis. **Laurent Duchêne:** Supervision, Formal analysis, Writing – review & editing. **Patrick Wheeler:** Supervision, Formal analysis, Review & editing.

Declaration of competing interest

The authors declare that they have no known competing financial interests or personal relationships that could have appeared to influence the work reported in this paper.

Data availability

Data will be available on demand.

Acknowledgments

The authors thank the support of ANID/ATE220023 Project; FONDECYT Regular Research Project 1220556; CLIMAT AMSUD 21001, FONDAP SERC Chile 1522A0006; International collaborative research project WBI/AGCID RI02 (DIE23-0001) and the University of Nottingham through the IRCF project 24932270.

References

[1] IRENA, Renewable capacity highlights-20, Irena (April) (2023) 3, https://www.irena.org/-/media/Files/IRENA/Agency/Publication/2022/Apr/IRENA_-RE_Capacity_Highlights_2022.pdf?la=en&hash=6122BF5666A36BECD5AAA2050B011ECE255B3BC7.

[2] IRENA, Renewable Capacity Statistics 2023, international Renewable Energy Agency, Abu Dhabi, IRENA, 2023, p. 69, https://www.irena.org/Publications/2023/Mar/Renewable-capacity-statistics-2023.

[3] V. Benda, L. Cerna, A note on limits and trends in PV cells and modules, Appl. Sci. 12 (7) (2022) http://dx.doi.org/10.3390/app12073363.

[4] I. Santiago, D. Trillo-Montero, I. Moreno-Garcia, V. Pallarés-López, J. Luna-Rodríguez, Modeling of photovoltaic cell temperature losses: A review and a practice case in South Spain, Renew. Sustain. Energy Rev. 90 (2018) 70–89, http://dx.doi.org/10.1016/j.rser.2018.03.054.

[5] D.D. Silva, V. Marson, R.R. de Souza, J.D. de Oliveira, J.B.C. Silva, E.M. Cardoso, A new predictive model for a photovoltaic module's surface temperature, Energy Rep. 8 (2022) 15206–15220, http://dx.doi.org/10.1016/j.egyr.2022.11.094.

[6] N. Aoun, Methodology for predicting the PV module temperature based on actual and estimated weather data, Energy Convers. Manag.: X 14 (2022) 100182, http://dx.doi.org/10.1016/j.ecmx.2022.100182.

[7] R.J. Mustafa, M.R. Gomaa, M. Al-Dhaifallah, H. Rezk, Environmental impacts on the performance of solar photovoltaic systems, Sustainability 12 (2) (2020) http://dx.doi.org/10.3390/su12020608.

[8] M.U. Siddiqui, O.K. Siddiqui, A.B. Alquaity, H. Ali, A.F. Arif, S.M. Zubair, A comprehensive review on multi-physics modeling of photovoltaic modules, Energy Convers. Manage. 258 (February) (2022) 115414, http://dx.doi.org/10.1016/j.enconman.2022.115414.

[9] L.D. Jathar, S. Ganesan, U. Awasarmol, K. Nikam, K. Shahapurkar, M.E.M. Soudagar, H. Fayaz, A. El-Shafay, M. Kalam, S. Bouadila, S. Baddadi, V. Tirth, A.S. Nizami, S.S. Lam, M. Rehan, Comprehensive review of environmental factors influencing the performance of photovoltaic panels: Concern over emissions at various phases throughout the lifecycle, Environ. Pollut. 326 (2023) 121474, http://dx.doi.org/10.1016/j.envpol.2023.121474.

[10] R. Kumar, M. Kumar, R. Gupta, Leakage current in solar photovoltaic modules, CRC Press, 2023, p. 111, http://dx.doi.org/10.1201/9781003373902-7.

[11] L.d. Santos, P.C.M. de Carvalho, C.d.C. Filho, Photovoltaic cell operating temperature models: A review of correlations and parameters, IEEE J. Photovolt. 12 (1) (2022) 179–190, http://dx.doi.org/10.1109/JPHOTOV.2021.3113156.

[12] A.U. Obiwulu, N. Erusiafe, M.A. Olopade, S.C. Nwokolo, Modeling and optimization of back temperature models of mono-crystalline silicon modules with special focus on the effect of meteorological and geographical parameters on PV performance, Renew. Energy 154 (2020) 404–431, http://dx.doi.org/10.1016/j.renene.2020.02.103.

[13] M. Koehl, M. Heck, S. Wiesmeier, J. Wirth, Modeling of the nominal operating cell temperature based on outdoor weathering, Sol. Energy Mater. Sol. Cells 95 (7) (2011) 1638–1646, http://dx.doi.org/10.1016/j.solmat.2011.01.020.

[14] M.E. Ya'acob, H. Hizam, T. Khatib, M.A.M. Radzi, C. Gomes, A.M. Bakri, M.H. Marhaban, W. Elmenreich, Modelling of photovoltaic array temperature in a tropical site using generalized extreme value distribution, J. Renew. Sustain. Energy 6 (3) (2014) 033134, http://dx.doi.org/10.1063/1.4885175.

[15] D. Evans, L. Florschuetz, Cost studies on terrestrial photovoltaic power systems with sunlight concentration, Sol. Energy 19 (3) (1977) 255–262, http://dx.doi.org/10.1016/0038-092X(77)90068-8.

[16] E. Skoplaki, J. Palyvos, On the temperature dependence of photovoltaic module electrical performance: A review of efficiency/power correlations, Sol. Energy 83 (5) (2009) 614–624, http://dx.doi.org/10.1016/j.solener.2008.10.008.

[17] M. Borunda, A. Ramírez, R. Garduno, G. Ruíz, S. Hernandez, O.A. Jaramillo, Photovoltaic power generation forecasting for regional assessment using machine learning, Energies 15 (23) (2022) http://dx.doi.org/10.3390/en15238895.

[18] A. Shafieian, M. Khiadani, A. Nosrati, Theoretical modelling approaches of heat pipe solar collectors in solar systems: A comprehensive review, Sol. Energy 193 (September) (2019) 227–243, http://dx.doi.org/10.1016/j.solener.2019.09.036.

[19] R. Ross, Interface design considerations for terrestrial solar cell modules, in: 12th Photovoltaic Specialists Conference, 1976, pp. 801–806, https://ui.adsabs.harvard.edu/abs/1976pvsp.conf..801R.

[20] H. Rauschenbach, Solar Cell Array Design Handbook, New York: Van Nostrand Reinhold Co, New York, 1980, https://refhub.elsevier.com/S0196-8904(23)00119-X/sb15.

[21] V. Risser, M. Fuentes, Linear regression analysis of flat-plate photovoltaic system performance data, in: 5th Photovoltaic Solar Energy Conference, 1984, pp. 623–627, https://ui.adsabs.harvard.edu/abs/1984pvse.conf..623R.

[22] T. Schott, Operation Temperatures of PV Modules: A Theoretical and Experimental Approach, 1985, pp. 392–396, https://pascal-francis.inist.fr/vibad/index.php?action=getRecordDetail&idt=8144674.

[23] R. Ross, M. Smokler, Electricity from photovoltaic solar cells Flat-Plate Solar Array Project final report. Volume VI: Engineering sciences and reliability, Technical Report October, JPL Publication, 86-31, Jet Propulsion Laboratory, California Inst. of Tech. United States, 1986, pp. 12–13, https://refhub.elsevier.com/S0196-8904(23)00119-X/sb18.

[24] F. Lasnier, T. Ang, Book Chapter: Chapter 6: Power Conditioning Systems, Routledge, 1990, Adam Hilger, Bristol and New York, Photovoltaic Engineering Handbook, https://refhub.elsevier.com/S2352-4847(22)02480-5/sb16.

[25] D.L. King, Photovoltaic module and array performance characterization methods for all system operating conditions, AIP Conf. Proc. 394 (1) (1997) 347–368, http://dx.doi.org/10.1063/1.52852.

[26] D.L. King, J.A. Kratochvil, W.E. Boyson, Field Experience with a New Performance Characterization Procedure for Photovoltaic Arrays, Technical Report, U.S. Department of Energy, 1997, p. 6, https://www.osti.gov/biblio/629484.

[27] G. Tamizhmani, L. Ji, Y. Tang, L. Petacci, C. Osterwald, Photovoltaic Module Thermal/Wind Performance: Long-Term Monitoring and Model Development For Energy Rating, 2003, pp. 936–939, https://refhub.elsevier.com/S0038-092X(22)00832-5/h0215.

[28] D.L. King, W.E. Boyson, J.A. Kratochvil, Photovoltaic Array Performance Model, Technical Report Sandia Report No. 2004-3535 8, U.S. Department of Energy, Springfield, 2004, pp. 1–19, http://dx.doi.org/10.2172/919131.

[29] J.A. Duffie, W.A. Beckman, Solar Engineering of Thermal Processes, John Wiley & Sons, 2013, https://refhub.elsevier.com/S0196-8904(23)00119-X/sb24.

[30] J.D. Mondol, Y.G. Yohanis, B. Norton, Comparison of measured and predicted long term performance of grid a connected photovoltaic system, Energy Convers. Manage. 48 (4) (2007) 1065–1080, http://dx.doi.org/10.1016/j.enconman.2006.10.021.

[31] E. Skoplaki, A. Boudouvis, J. Palyvos, A simple correlation for the operating temperature of photovoltaic modules of arbitrary mounting, Sol. Energy Mater. Sol. Cells 92 (11) (2008) 1393–1402, http://dx.doi.org/10.1016/j.solmat.2008.05.016.

[32] A.M. Muzathik, Photovoltaic modules operating temperature estimation using a simple correlation, Int. J. Energy Eng. 4 (August 2014) (2014) 151–158, https://api.semanticscholar.org/CorpusID:113931662.

[33] W.C.L. Kamuyu, J.R. Lim, C.S. Won, H.K. Ahn, Prediction model of photovoltaic module temperature for power performance of floating PVs, Energies 11 (2) (2018) http://dx.doi.org/10.3390/en11020447.

[34] S. Jacques, Chapter five the importance of cell temperature in modelling the energy efficiency, Cambridge Scholars Publishing, 2020, p. 67, https://univ-tours.hal.science/hal-02525736.

[35] P. Bevilacqua, S. Perrella, R. Bruno, N. Arcuri, An accurate thermal model for the PV electric generation prediction: long-term validation in different climatic conditions, Renew. Energy 163 (2021) 1092–1112, http://dx.doi.org/10.1016/j.renene.2020.07.115.

[36] S. Kaplanis, E. Kaplani, J. Kaldellis, PV temperature and performance prediction in free-standing, BIPV and BAPV incorporating the effect of temperature and inclination on the heat transfer coefficients and the impact of wind, efficiency and ageing, Renew. Energy 181 (2022) 235–249, http://dx.doi.org/10.1016/j.renene.2021.08.124.

[37] G.G. Kim, J.H. Choi, S.Y. Park, B.G. Bhang, W.J. Nam, H.L. Cha, N. Park, H.-K. Ahn, Prediction model for PV performance with correlation analysis of environmental variables, IEEE J. Photovolt. 9 (3) (2019) 832–841, http://dx.doi.org/10.1109/JPHOTOV.2019.2898521.

[38] D.P.N. Nguyen, K. Neyts, J. Lauwaert, Proposed models to improve predicting the operating temperature of different photovoltaic module technologies under various climatic conditions, Appl. Sci. 11 (15) (2021) http://dx.doi.org/10.3390/app11157064.

[39] O.O. Yolcan, R. Kose, Photovoltaic module cell temperature estimation: Developing a novel expression, Sol. Energy 249 (2023) 1–11, http://dx.doi.org/10.1016/j.solener.2022.11.020.

[40] M.A. Rahaman, T.L. Chambers, A. Fekih, G. Wiecheteck, G. Carranza, G.R.C. Possetti, Floating photovoltaic module temperature estimation: Modeling and comparison, Renew. Energy 208 (2023) 162–180, http://dx.doi.org/10.1016/j.renene.2023.03.076.

[41] R. Korab, M.P. omski, T. Naczyński, T. Kandzia, A dynamic thermal model for a photovoltaic module under varying atmospheric conditions, Energy Convers. Manage. 280 (2023) 116773, http://dx.doi.org/10.1016/j.enconman.2023.116773.

[42] IEC, Terrestrial photovoltaic (PV) modules – Design qualification and type approval – Part 1-1: Special requirements for testing of crystalline silicon photovoltaic (PV) modules, ISBN: 2831886376, 2021, IEC 61215-1-1:2021, https://webstore.iec.ch/publication/61346.

[43] L. Amodeo, E.-G. Talbi, F. Yalaoui, Recent Developments in Metaheuristics, vol. 62, Springer International Publishing AG 2018, 2018, pp. 219–225, http://dx.doi.org/10.1007/978-3-319-58253-5.

[44] E. Osaba, E. Villar-Rodriguez, J. Del Ser, A.J. Nebro, D. Molina, A. LaTorre, P.N. Suganthan, C.A. Coello Coello, F. Herrera, A tutorial on the design, experimentation and application of metaheuristic algorithms to real-world optimization problems, Swarm Evol. Comput. 64 (2021) 100888, http://dx.doi.org/10.1016/j.swevo.2021.100888.

[45] Q. Liu, X. Li, H. Liu, Z. Guo, Multi-objective metaheuristics for discrete optimization problems: A review of the state-of-the-art, Appl. Soft Comput. 93 (2020) 106382, http://dx.doi.org/10.1016/j.asoc.2020.106382.

[46] M. Agnoletti, Y.M. Pelegrín, A.G. Alvarez, The traditional agroforestry systems of Sierra del Rosario and Sierra Maestra, Cuba, in: Biodiversity and Conservation, vol. 31, Springer Netherlands, 2022, pp. 2259–2296, http://dx.doi.org/10.1007/s10531-021-02348-8.

[47] C.F. Rivera, M.M. Alvarez, M.H. González, R.P. Suárez, B.V. Saldívar, N.V. Figueredo, I.G. García, V.C. Cancino, R.V. Montenegro, E. Beatriz, C. Estopiñan, I.M. Arenal, A.H. Mayo, J.C. Infante, B.L. Pedroso, O.M. Lobaina, Y.R. Ortega, State of the climate in Cuba 2022. Extended summary, Revista Cubana de Meteorología 29 (1) (2023) 1–16, https://rcm.insmet.cu/index.php/rcm/article/view/703.

[48] E. Alberto Alvarez, M. Korkeakoski, A. Santos Fuentefrí a, M. Lourdes Filgueiras Sainz de Rozas, R. Arcila Padura, J. Luukkanen, Long-range integrated development analysis: The Cuban Isla de la Juventud study case, Energies 14 (10) (2021) http://dx.doi.org/10.3390/en14102865.

[49] J. Morales Pedraza, Solar energy in Cuba: Current situation and future development, J. Solar Energy Res. Updates 6 (2019) 1–14, http://dx.doi.org/10.31875/2410-2199.2019.06.1.

[50] M. Korkeakoski, Towards 100% renewables by 2030: Transition alternatives for a sustainable electricity sector in Isla de la Juventud, Cuba, Energies 14 (10) (2021) http://dx.doi.org/10.3390/en14102862.

[51] E. Iakovleva, D. Guerra, P. Tcvetkov, Y. Shklyarskiy, Technical and economic analysis of modernization of solar power plant: A case study from the Republic of Cuba, Sustainability 14 (2) (2022) http://dx.doi.org/10.3390/su14020822.

[52] J. McFadden, Razor sharp: The role of Occam's razor in science, Ann. New York Acad. Sci. 1530 (1) (2023) 8–17, http://dx.doi.org/10.1111/nyas.15086.

[53] CCE, Serie DSM-270. Energía Solar. Anexo No. 3, 2023, p. 2, www.cce.cu/uploads/ficha/Especificaciones%20T%C3%A9cnicas%20DSM-270_actualizada.pdf.

[54] JinkoSolar, Eagle 60P 265-285 Watt. Poly Crystalline Module, 2023, p. 2, www.jinkosolar.com/uploads/Eagle%20JKM265-285PP-60-(V)-A3,1-EN.pdf.

[55] M. Abdel-Basset, L. Abdel-Fatah, A.K. Sangaiah, Chapter 10 - metaheuristic algorithms: A comprehensive review, in: A.K. Sangaiah, M. Sheng, Z. Zhang (Eds.), Computational Intelligence for Multimedia Big Data on the Cloud with Engineering Applications, in: Intelligent Data-Centric Systems, Academic Press, 2018, pp. 185–231, http://dx.doi.org/10.1016/B978-0-12-813314-9.00010-4.

[56] M. Muller, Measuring and Modeling Nominal Operating Cell Temperature, NOCT, Technical Report. National Renewable Energy Laboratory, 2010, https://refhub.elsevier.com/S0306-2619(22)01090-X/sb6.

[57] E.-G. Talbi, Metaheuristics: from Design to Implementation, John Wiley & Sons, 2009, https://refhub.elsevier.com/S0377-2217(22)00127-8/sbref0094.

[58] F. Hillier, G. Lieberman, Introduction to Operations Research, eleventh ed., McGraw-Hill Education, 2021, p. 964, https://books.google.be/books?id=1gNMygEACAAJ.

[59] D. Chalupa, P. Nielsen, Parameter-free and cooperative local search algorithms for graph colouring, Soft Comput. 25 (24) (2021) 15035–15050, http://dx.doi.org/10.1007/s00500-021-06347-3.

[60] X.-L. Jing, Q.-K. Pan, L. Gao, Local search-based metaheuristics for the robust distributed permutation flowshop problem, Appl. Soft Comput. 105 (2021) 107247, http://dx.doi.org/10.1016/j.asoc.2021.107247.

[61] A. Barredo Arrieta, N. Díaz-Rodríguez, J. Del Ser, A. Bennetot, S. Tabik, A. Barbado, S. Garcia, S. Gil-Lopez, D. Molina, R. Benjamins, R. Chatila, F. Herrera, Explainable Artificial Intelligence (XAI): Concepts, taxonomies, opportunities and challenges toward responsible AI, Inf. Fusion 58 (2020) 82–115, http://dx.doi.org/10.1016/j.inffus.2019.12.012.

[62] Bharadwaj, K.B. Prakash, G.R. Kanagachidambaresan, Programming with TensorFlow: Solution for Edge Computing Applications, Springer International Publishing, Cham, 2021, pp. 105–144, http://dx.doi.org/10.1007/978-3-030-57077-4_11.

[63] B.J. Smucker, N.T. Stevens, J. Asscher, P. Goos, Profiles in the teaching of experimental design and analysis, J. Stat. Data Sci. Educ. (2023) 1–14, http://dx.doi.org/10.1080/26939169.2023.2205907.

[64] P. Dwivedi, K. Sudhakar, A. Soni, E. Solomin, I. Kirpichnikova, Advanced cooling techniques of P.V. modules: A state of art, Case Stud. Therm. Eng. 21 (December 2019) (2020) 100674, http://dx.doi.org/10.1016/j.csite.2020.100674.

[65] W. Luo, Y.S. Khoo, P. Hacke, V. Naumann, D. Lausch, S.P. Harvey, J.P. Singh, J. Chai, Y. Wang, A.G. Aberle, S. Ramakrishna, Potential-induced degradation in photovoltaic modules: A critical review, Energy Environ. Sci. 10 (1) (2017) 43–68, http://dx.doi.org/10.1039/c6ee02271e.